Adsorption and Disproportionation of Carbon

Monoxide on Faceted-Gold Surfaces and Edges

David Khayata, Gil M. Repa, Lisa A. Fredin*

Department of Chemistry, Lehigh University, Bethlehem, Pennsylvania 18015, USA.

*lafredin@lehigh.edu

Abstract. Localized surface plasmons (LSP) on faceted surfaces of gold nanoparticles enable

carbon monoxide disproportionation to be driven at room temperature. In order to expand the

known surfaces that catalyze this reaction, we explore the adsorption of carbon dioxide at top, long

bridge, short bridge, and hole sites on gold (100), (110), (111), (211), and (311) faceted surfaces,

as well as the reaction barriers for disproportionation at the lowest energy adsorption site on each

surface and edges between two (311) surfaces and (100) and (110) surfaces. Generally, the less

atomically dense higher index facets promote both good adsorption and reactivity, and the edges

show lower barriers for disproportionation. For most of the explored surfaces, adsorption directly

on top of a gold atom is most favorable. The lowest activation energy for carbon monoxide

disproportionation to amorphous carbon and carbon dioxide is predicted for two carbon monoxides

adsorbed on top of atoms on the (311)/(311) edge.

Keywords. Quantum mechanics, catalysis, gold nanoparticles, local surface plasmon, CO

disproportionation.

1

1. Introduction

The controlled decomposition of carbon monoxide (CO) provides a way to generate amorphous carbon[1,2] from industrially generated CO rather than allowing its release. The disproportionation of carbon monoxide (eqn. 1) typically takes place between 400 °C and 600 °C in industrial settings, [2,3] often with the help of metal catalyst. Different transition metal surfaces have been explored to improve the efficiency of CO decomposition, including iron, [4,5] aluminum/iron, [6] copper [7], and metal-oxides [8]. Each of these catalysts still require significant temperature or pressure [9] to drive the reaction. However, the reaction can also be mediated by light-induced localized surface plasmons (LSPs) on gold nanoparticles at room temperature [1,10,11].

$$2CO(g) \rightarrow C(s) + CO_2(g) \tag{1}$$

The LSP originates from the confinement of light in metallic nanoparticles, which induces collective motion of many electrons in unison at the material interface [12]. The LSP provides "hot" electrons or extra energy that can catalyze CO conversion [1,13–15]. The ability to drive CO disproportionation with light at room temperature provides a new level of control over the reaction, possibly minimizing side products and enabling direct CO catalysis at the source without needing to provide or contain large amounts of heat. These properties provide opportunities to expand CO decomposition in more diverse applications like car exhaust and ventilation systems.

The initial demonstration of CO disproportionation on gold [1] revealed that favorable adsorption locations of the CO and the localization of the LSP energy are critical factors for the generation of amorphous carbon. The initial computational analysis provided insights only into the adsorption of CO directly on top of a gold atom on the (100), (110), and (311) surfaces [1,16]. Other low index facets have also been previously studied for CO adsorption experimentally and computationally [17–23], however these studies focus on adsorption energies as a proxy of

reactivity. While a strong adsorption of the reactant can promote the required association to start the reaction, it is clear that the complex interplay of electronic factors along the reaction profile are still critical to study for each reaction because the most stable adsorption energies do not always translate to the most reactive surfaces [1,23–27]. In fact, the initial demonstration of this reaction [1] concluded that the location of the reactivity was driven mostly by the LSP concentration.

Here, we further explore adsorption and reactivity directly on these and other low index facets to better understand the role of thermodynamics in the reactivity and find additional reactive gold surfaces that could guide design of new catalytic particles for CO conversion. This work focuses on the (100), (110), (111), (211), and (311) gold surfaces, as well as the top, bridge, and hole sites of each surface. Both the adsorption energy and decomposition of CO on each surface are calculated using density functional theory (DFT). In particular, this work not only identifies more adsorption sites, but also directly compares disproportionation reaction barriers of two neighboring CO molecules using nudged elastic band (NEB) [28] to explore the potential energy surface of this reaction directly. In addition, the facet edges that were measured to be reactive in ref. [1] are explored to investigate the difference in catalytic mechanism between facets and edges. By mapping possible catalytic sites on a range of gold facets and edges, the fundamental properties of adsorption sites that promote reactivity are characterized.

2. Theoretical Methods

Each surface slab was obtained by cutting the gold surface of interest into the smallest possible orthorhombic unit cell. Unit cells were constructed such that at least 15 Å of vacuum space separated periodic images to prevent artificial interactions. Carbon monoxide was added on chosen sites (e.g., top, bridge, long bridge, and hole) and optimized.

First-principles calculations using spin-polarized DFT in Quantum ESPRESSO [28] were performed in order to determine the lowest energy adsorption on each of the surface sites. Spin polarization was used to allow spin to localize to the adsorbates and more accurately model the reaction mechanism [29]. The generalized gradient approximation (GGA) of Perdew–Burke-Ernzerhof (PBE) [30] and ultrasoft psuedopotentials were used for all optimizations [31]. The optimizations were converged to a force less than 0.05 eV/Å using a k-point grid of 10 x 10 x 1 in the Monkhorst-Pack scheme. The criterion for electronic convergence was set at 10⁻⁶ Ry. A kinetic energy cutoff of the wave functions of 40 eV and augmentation charge of 240 eV were required to converge all surfaces with adsorbates with respect to the size of the basis. Final energy calculations were accomplished using the hybrid HSE06 [32,33] functional, which has been specifically designed to be computationally efficient with periodic systems and providing more accurate electronic structures.

NEB [34,35] was used to obtain the minimal energy path (MEP) between the reactants (2 CO molecules) and the products (adsorbed carbon and a free CO₂). The initial image is 2 CO molecules optimized on the same surface site (*e.g.*, top) and the final image is an adsorbed carbon atom and a CO₂ molecule > 2.5 Å from the surface. The seven-image MEP obtained from the NEB calculation was then used to construct a reaction energy profile for the different surfaces. To achieve a path convergence threshold of 100 meV/Å, the NEB calculations required a higher kinetic energy cutoff of the wave functions of 60 eV, with a corresponding augmentation charge of 480 eV and a 10 x 10 x 1 k-point mesh. For calculation of the MEP on the (110)/(100) and (311)/(311) edge structures, the Vienna Ab Initio Simulation (VASP)[36] program was employed. This set up mirrored those conditions described above, utilizing the projector augmented wave (PAW) method [37] with the following core/valence configurations: Au:[Xe]4f/5d6s, C:[He]/2s2p,

O:[He]/2s2p. Zero-point energy and entropic contributions at 298.15 K were calculated using VASPKIT [38]. Frequencies were derived from perturbation theory where the Au atoms were frozen and

only the adsorbate molecules were calculated, which is a reasonable approximation considering the large mass difference between the metal and adsorbed atoms.

3. Results and Discussion

3.1 Surface Adsorption of Carbon

Monoxide

CO adsorption was considered on top of a surface Au atom, in surface holes (hollows between more than 2 atoms), and bridging two surface atoms, on the (100), (110), (111), (211), and (311) Au surfaces (Table S1), with adsorption being generally favorable (Table 1). The adsorption energies and structures are very similar to other reported calculations [23,39–42]. The PBE (Table S2) adsorption energies match those reported for CO adsorption using PBE [23,39,41] and PW91 [40,42,43] functionals. Previous work showed HSE06 adsorption energies slightly higher than those for PBE across a range of Au

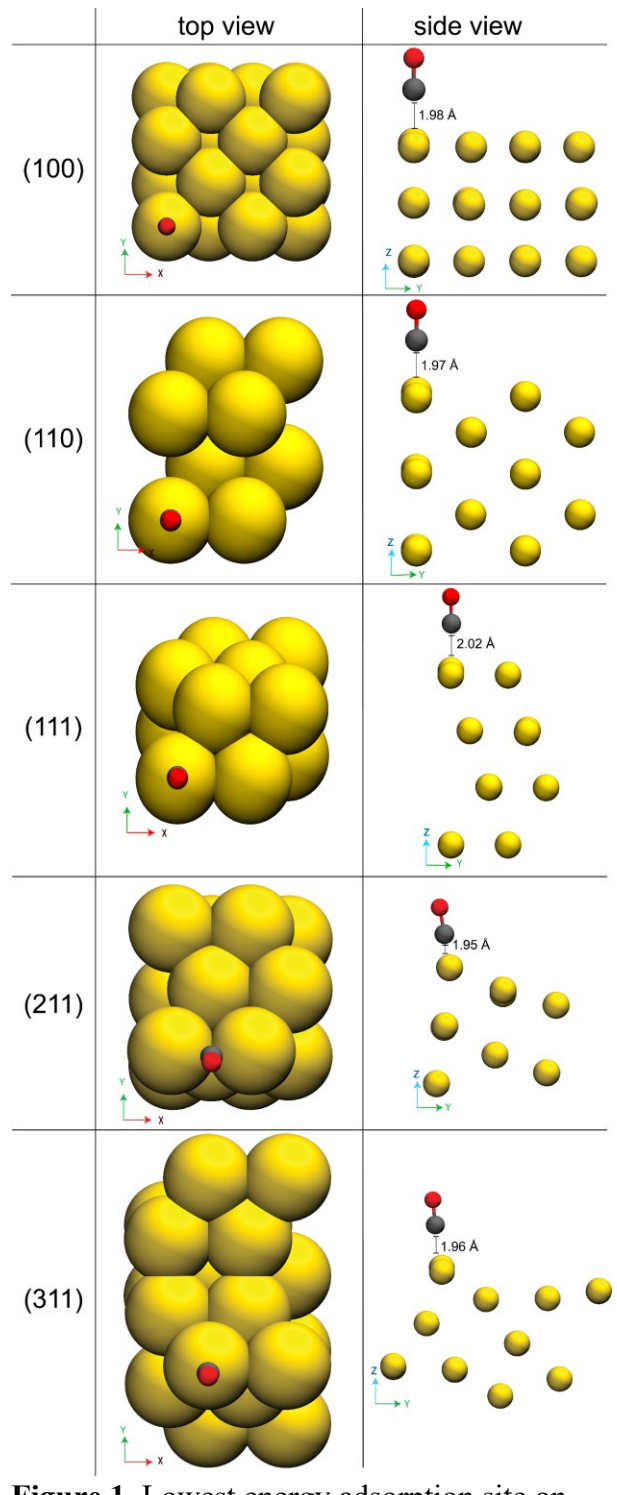


Figure 1. Lowest energy adsorption site on each Au facet. All sites studied are summarized in Table 1 and Figures S1-S5.

coordination number [44]. Our HSE06 energies (Table 1) show the same adsorption favorability ordering as PBE (Table S2) but the actual energies shift to more stability for the most favorable adsorption geometries, with only the least favorable structures showing higher energies at the HSE06 level of theory. This shows that the adsorption of CO on gold is a complex electrostatic interaction that requires a well localized electron density to accurately describe [45]. For most surfaces, the most stable adsorption (E_{ads}, eqn. 2, Table 1) occurs on top of an atom (

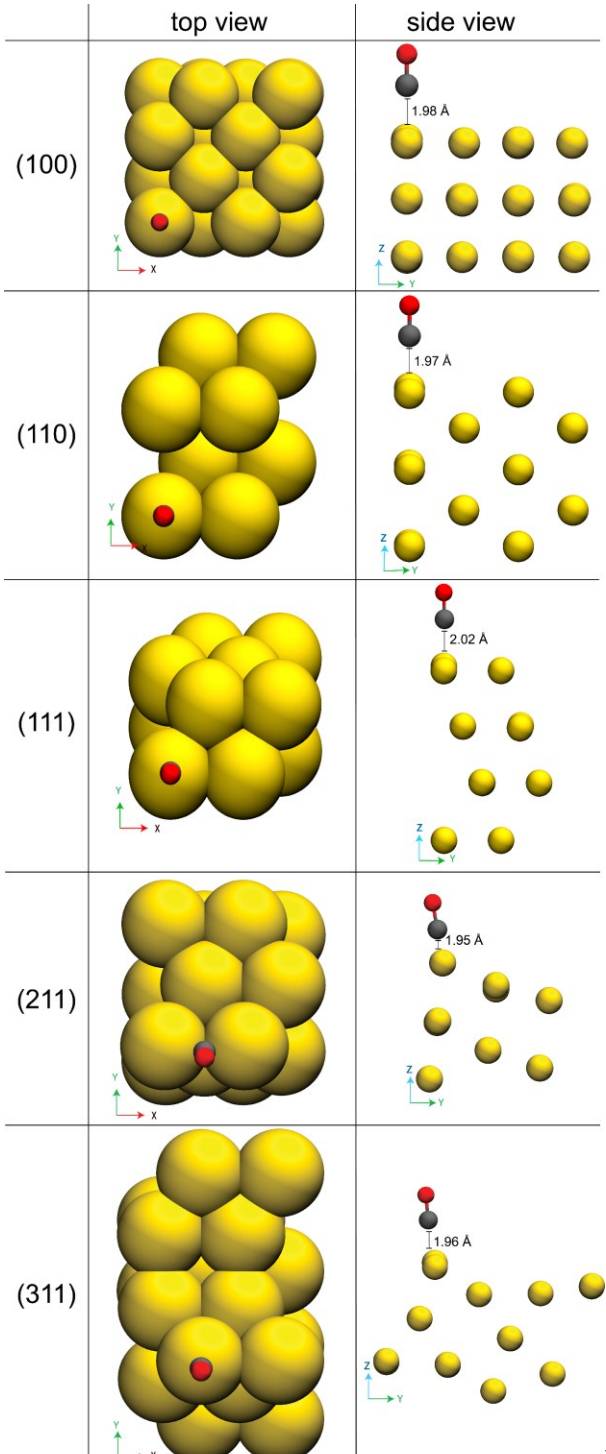


Figure 1) except on the (211) surface where the

short bridge (Figure S4) between neighboring surface atoms is slightly more favorable (Table 1). The top site is highly favorable due to the stronger interaction between the CO and a single surface atom compared to the bridging and hole sites. The CO is closer to the surface in most bridge sites,

(Figures S2-S6) however it is still \sim 2 Å from the nearest Au atoms as it is between two surface sites.

$$E_{ads} = E_{slab+CO} - E_{slab} - E_{CO} \tag{2}$$

Au (100) and (111) are the densest surfaces with no hole sites large enough to accommodate CO adsorption on the surface. On these surfaces the top adsorption is clearly favored (Table 1). In contrast, the stability of (110) sites switch order between PBE and HSE06 (Table S2). The top site is favored by PBE, but the hybrid description predicts the top and short bridge nearly isoenergetic. The long bridge starting geometry optimizes the CO closer to one Au surface atom (Table S2) making it unrepresentative.

Au (110), (211), and (311) facets have wider spaced surface atoms that seem to stabilize adsorption of CO at those sites in which the CO interacts with multiple surface atoms, e.g., bridging

and hole sites. This contributes to the fact that the short bridge and hole sites are nearly degenerate on the (211) surface at -1.01 and -1.03 eV, respectively. Previous calculations focused solely on the bridge sites of (211) confirming the preference for adsorption of CO not at top sites. [40,42,43] Both sites are more favorable than the top site on the (211) surface (Table 1). In both the short bridge and hole binding, the CO's close interaction with the surface results in surface reconstruction that stabilizes the multi-atom (Au–C–Au)

Table 1. The HSE06 adsorption energies for one adsorbed CO molecule per unit cell.

surface	site	energy (eV)
(100)	top	-3.88
	short bridge	0.39
(110)	top	-1.15
	short bridge	-1.21
	long bridge	-1.16
	hole	-0.02
(111)	top	-0.62
	long bridge	-0.28
	bridge	0.02
(211)	top	-0.70
	hole	-1.03
	long bridge	0.57
	short bridge	-1.01
(311)	top	-1.01
	long bridge	0.18
	short bridge	-0.59

interaction. Such an effect is also observed on the (311) surface, where short bridge binding is favorable at -0.59 eV. Binding at the long bridge on this surface is unfavorable. Top site binding on the (311) surface remains the most favorable at -1.01 eV.

3.2 Disproportionation Reactivity

After the preferred adsorption sites for CO were identified for each surface, the MEP and transition state for CO disproportionation (eqn. 1) were determined. Often adsorption is used as a measure of the reactivity of particular surfaces but this often does not correctly order the reactivity of surfaces, indicating that it misses nuances in the reaction mechanism. While it is clear that the CO disproportionation on gold requires the LSP, there is still debate about if the LSP provides "hot" electrons, driving the reaction through a reduction pathway, or extra energy, like a traditional catalyst, or through some more complex excited state processes [1,13–15]. In initial calculations of reduced CO adsorbed unit cells (i.e. adding an additional electron to the unit cell) showed that they were less stable than the ground state structure. In fact, in optimizations of reduced unit cells the CO often moved away from the Au surface indicating an unfavorable reaction. Thus, rather than exploring a reduction mechanism, this work focuses on the thermodynamics of the gold surfaces acting like a traditional catalyst that allows reactions with higher barriers to occur. As nano-Au LSP energies have been measured to be $\sim 2-4$ eV [1,46], we assume that reaction energies and barriers in this range are reasonable. Excited state pathways would require multireference computational methods beyond DFT.

The reaction barriers for two adsorbed COs were determined for all sets of "nearest neighbor" sites of the lowest energy adsorption site (Figure S7). While not every NEB-calculated path

proceeds by both CO molecules tilting towards the surface until the oxygen of one CO binds to the C of the other, followed by a linear CO₂ moving away from the surface. Previous studies have focused on CO₂ adsorption on gold surfaces but then the CO₂ is kept close to the surface to find a maximum interaction, here the CO₂ is at least 2 Å from any Au atoms. The oxygen transfer occurs when the two CO molecules either align linearly (211) or in a V-shaped geometry (110, 111, 311) in the transition states (Figure 2, top view) depending on how far the adsorption sites are from each other, with V-shaped being driven by closely adsorbed COs.

On the (110) surface there are two nearest neighbor top sites: one set along the x-axis where the Au atoms are 4.08 Å apart and one along the y-axis 2.88 Å apart.

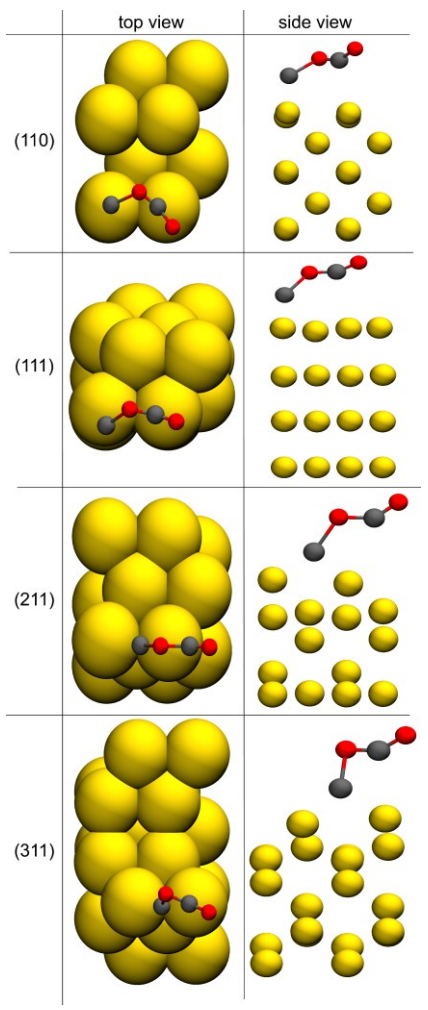


Figure 2. Transition states for CO disproportionation on each surface. Full paths are shown in Figures S7-S12.

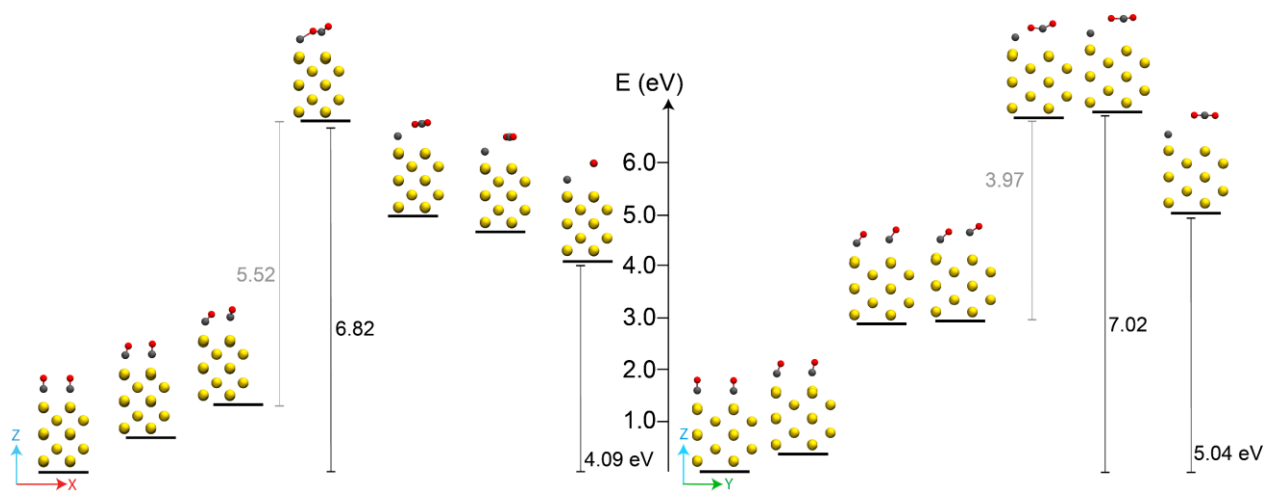


Figure 3. The HSE06 energy profile of the reaction $2CO_{(g)} \rightarrow C_{(s)} + CO_{2(g)}$ on the (110) nearest neighbor top sites along the x-axis (4.078 Å apart, left) and y-axis (2.884 Å apart, right). Each image geometry is seen from the side to show the overall reaction pathway, larger images (Figures S7 & S8) and top views of CO adsorption geometries (Figure S6) and the transition states (Figure 2), support the same mechanism.

Formation of the new C–O bond requires an energy barrier of 3.97 or 5.52 eV for adsorption along the x- and y-axis respectively (Figure 3). Subsequent dissociation of the CO_2 releases ~ 2 eV. The

overall reaction on the (110) surface is endothermic with fairly high activation energy (> 5.5 eV), which is higher than the typical Au LSP 2 energy eV) [1,46]. We were unable to optimize the reaction profile on the (110) short

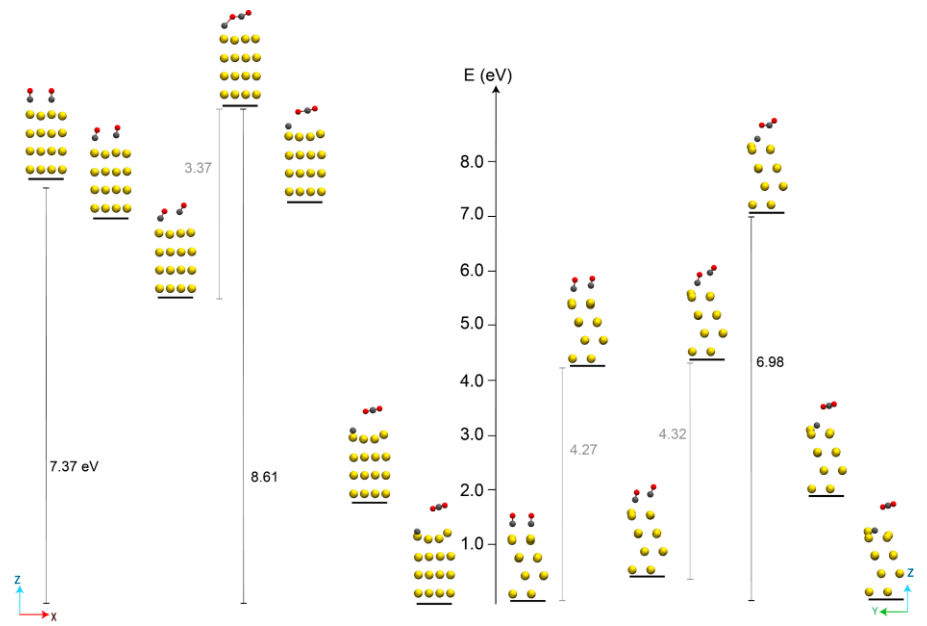


Figure 4. The HSE06 energy profile of the reaction $2CO_{(g)} \rightarrow C_{(s)} + CO_{2(g)}$ on the (111) nearest neighbor top sites along the x-axis (2.884 Å apart, left) and the x+30° diagonal (4.96 Å apart, right). Each image geometry is seen from the side to show the overall reaction pathway, larger images (Figures S9 & S10) and top views of CO adsorption geometries (Figure S6) and the transition states (Figure 2), support the same mechanism.

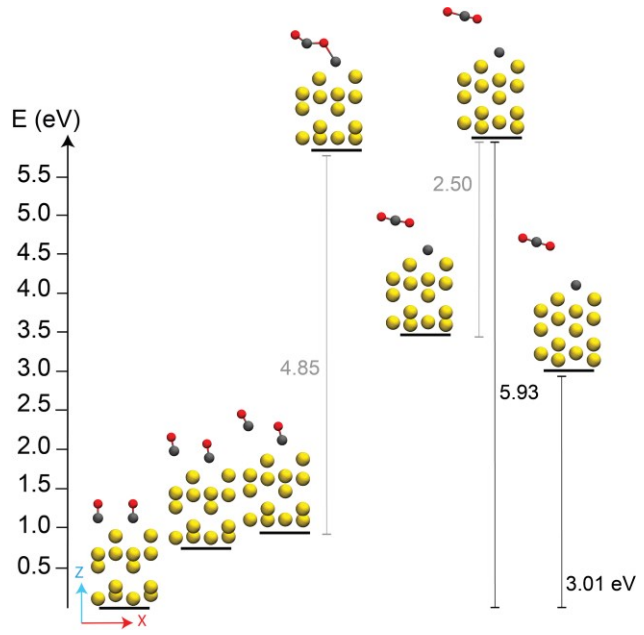


Figure 5. The HSE06 energy profile of the reaction $2CO_{(g)} \rightarrow C_{(s)} + CO_{2(g)}$ on the (211) nearest neighbor bridge sites along the x-axis (2.88 Å apart). Each image geometry is seen from the side to show the overall reaction pathway, larger images (Figures S11) and top views of CO adsorption geometries (Figure S6) and the transition states (Figure 2), support the same mechanism.

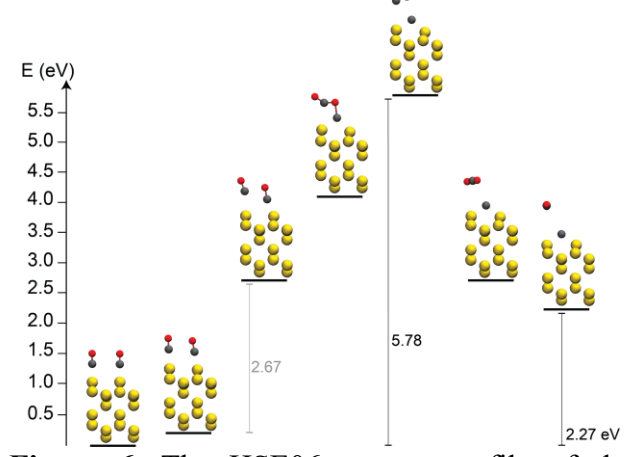


Figure 6. The HSE06 energy profile of the reaction $2CO_{(g)} \rightarrow C_{(s)} + CO_{2(g)}$ on the (311) nearest neighbor top sites along the x-axis (3.08 Å apart). Each image geometry is seen from the side to show the overall reaction pathway, larger images (Figures S12) and top views of CO adsorption geometries (Figure S6) and the transition states (Figure 2), support the same mechanism.

bridge sites due to the large unit cell needed for convergence. However, the short bridge Au–Au and Au–C distances on the (110) surface are very similar for to the short bridge on the (211) facet, and therefore the (110) short bridge reactivity is expected to look similar to the (211) reaction profile.

On the (111) surface, the two nearest neighbor top sites are along the x-axis (Au atoms 2.88 Å apart) and along the x+30° diagonal (4.96 Å apart, Figure 4). In both reaction paths, the carbon product embeds into the surface rather than remaining on the top site. Multiple product geometries were optimized to attempt to find a structure where the carbon remained on the surface. However, in each case the carbon embeds itself between surface atoms. This is interesting since the (111) surface is a particularly dense Au surface (0.119 Au/Å, Table S1). While one might expect this embedding to be unfavorable, this optimized structure is lower in energy than the two

adsorbed COs by ~ 5 and ~ 10 eV with PBE and HSE06, respectively (Table S2). The ~ 2 Å difference in the starting CO positions leads to a significant difference in the barrier to forming the new C–O bond ($\Delta\Delta E_a \sim 2$ eV). However, both MEPs show high variability in the energies of each image due to very slight structural changes of the surface Au atoms, indicating that computational models may not be able to describe the reactivity of this surface.

The disproportionation on adjacent (211) short bridge sites (Figure 5) is similar to those on the top sites of other surfaces. However, the high energy transition state in which the new C–O bond is formed is the most linear of those predicted here (Figure 2). The barrier on this surface is slightly lower than most of those for the lower index facets, indicating that the less dense, higher index facets promote both good adsorption and reactivity. This is not totally surprising, as binding energy has been seen to correlate with surface atom coordination number in small gold clusters, with lower

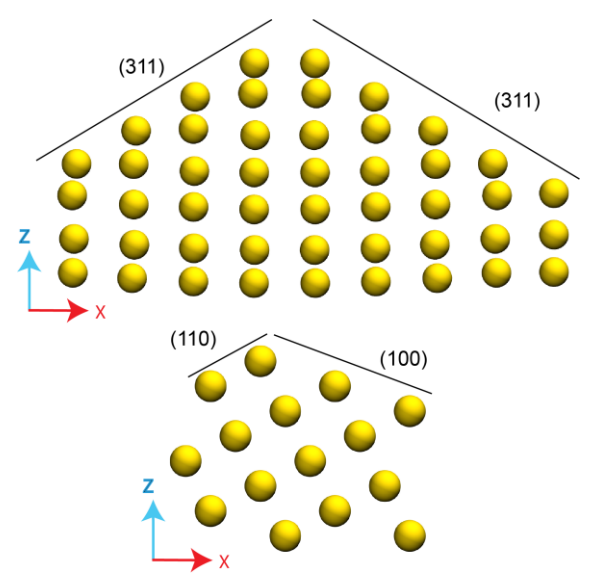


Figure 7. Edge unit cells with the exposed surfaces labeled.

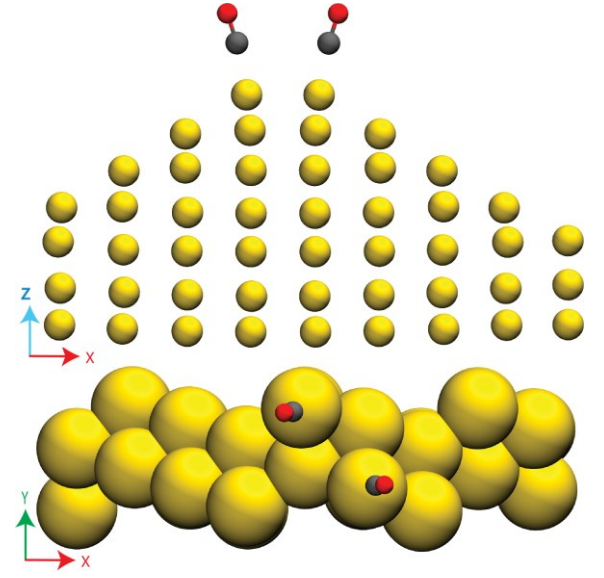


Figure 8. (311)/(311) edge with two adsorbed COs on nearest neighbor top sites.

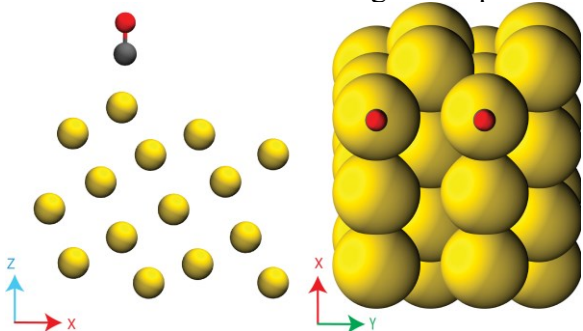


Figure 9. (110)/(100) edge with two adsorbed COs on nearest neighbor top sites

coordination leading to more favorable binding [47–49].

The reaction barrier to disproportionation on the (311) surface is intermediately sized among those calculated here. The reaction on this surface proceeds through a different mechanism (Figure S12) where the two COs tilt in opposite directions, forming a ~ 41° dihedral between the O–C–O–C (Figure 2) before one of the oxygen atoms jumps ~ 0.7 Å to form the new C–O bond (Figure 6). While the absolute energy of each of these reaction barriers is higher than the typical Au LSP, the relative trends reveal that the adsorption is most stable on (311), (211), and (110) surfaces and the reaction is most probable on the (211) surface.

3.3 Modeling Au particle edges

LSP builds up at corners and edges of prism particles based on their symmetry [1,50–52]. In order to understand if the edges of the particle are naturally more reactive because of undercoordination or because of the higher energy of the LSP in these areas, we built edge models for both the (311)/(311) and (110)/(100) intersections (Figure 7). Repeatable units for each edge resulted in a longer x-axis for the (311)/(311) edge (Figure S13) and a longer y-axis for the (110)/(100) (Figure S14). The (311)/(311) edge is two ridges of atoms running along the y-axis, whereas the (110)/(100) edge has a single atom wide ridge along the y-axis of the unit cell. Adsorption of two COs on the closest edge atoms optimize to ~ 1.9 Å above the edge on both surfaces, but the two COs are 0.5 Å further apart on the (311)/(311) edge (Figure 8) than the (110)/(100) edge (Figure 10) because the nearest neighbor Au atoms are diagonal on the (311)/(311) edge.

3.4 Edge Reactivity

The MEP for the $2CO_{(g)} \rightarrow C_{(s)} + CO_{2(g)}$ reaction was optimized on each edge (Figure 10 & Figure 11), starting from two COs adsorbed on the closest edge sites for each edge. No true transition

state was found in either NEB path despite multiple attempts or adding additional images between the initially optimized steps. It is important to note that the energies for both edge reactions are given from the PBE SCF paths the the (311)/(311)edge did not converge with HSE06. The edge unit cells have the minimum number of atoms to generate a repeatable unit to minimize computational cost. This resulted in the (311)/(311) edge having a y-axis that is only 4.97 Å long. Because this axis is shorter than the range separation parameter in

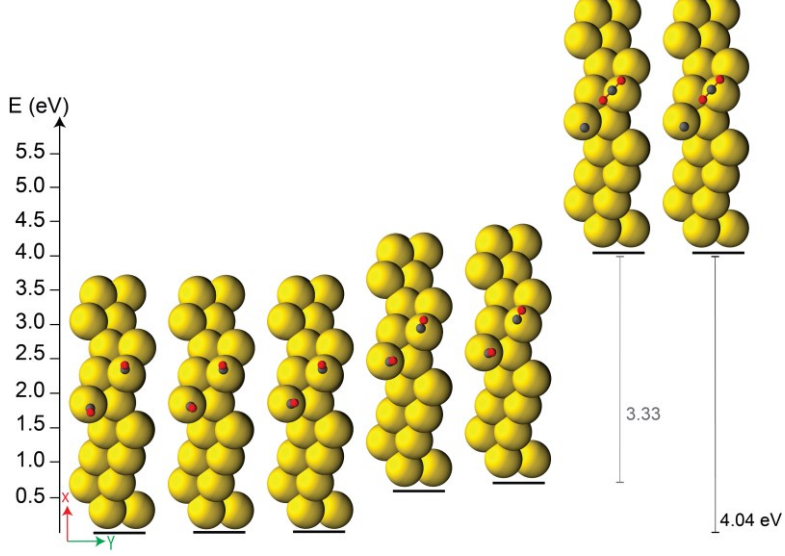


Figure 10. The PBE energy profile of the reaction $2CO_{(g)} \rightarrow C_{(s)} + CO_{2(g)}$ on the (311)/(311) nearest neighbor top sites along the y-axis (4.55 Å apart). Each image geometry is seen from the top to show the overall reaction pathway, side images (Figures S15) support the same mechanism.

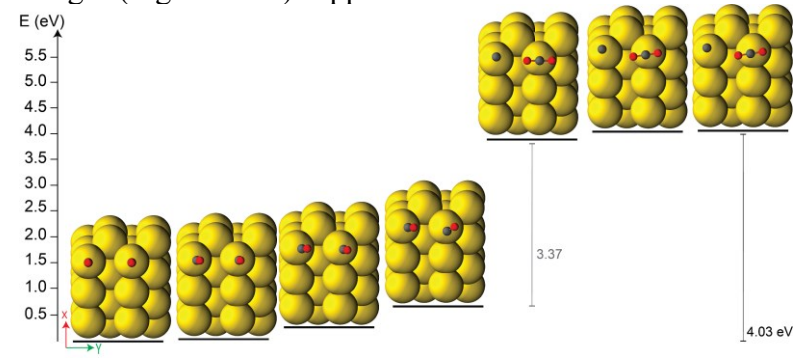


Figure 11. The PBE energy profile of the reaction $2CO_{(g)} \rightarrow C_{(s)} + CO_{2(g)}$ on the (110)/(100) nearest neighbor top sites along the y-axis (4.08 Å apart). Each image geometry is seen from the top to show the overall reaction pathway, side images (Figures S16) support the same mechanism.

HSE06 and because the reaction was occurring along this axis the HSE06 energies of the images did not converge. We tried both using a 2x1x1 unit cell of the slab and decreasing the convergence criteria. The NEB MEP didn't converge for the large unit cell with almost 2 months of runtime. Even with a lower converged solution as a starting guess, we were unable to get a reasonable

converged electronic solution using HSE06. However, like all the faceted reactions, the energy differences along the path changed very little with HSE06 for the (110)/(111) edge (Table S8).

Each MEP shows the formation of the new C–O bond to generate CO_2 is nearly isoenergetic with the final products. The activation barriers are both ~ 3.3 eV; much lower than those seen on the flat facets, and well within the LSP energy that is measured on these types of edges. The barrier for the reaction on the (311)/(311) edge is slightly lower so it would be expected to be more reactive. Electron energy loss spectra (EELS) of these particles indicate that experimentally carbon accumulates on only the (110)/(100) edge of a titania supported particle [1]. Analytical models of the LSP indicated that the buildup comes from the orientation of the particles on the titania, as the edges with the highest electrostatic interaction with the titania, the (311)/(311) in the prismatic particle [1], preferentially lay along the surface of the support reducing their catalytic activity. The free particles would therefore be expected to be more reactive on all edges. Or to take advantage of the inherent catalytic properties of the edges, particles that orient on a support with all edges free should be designed.

4. Conclusions

Here the reactivity of CO disproportionation is explored on a range of gold surface sites directly. The adsorption energies are predicted for a single CO on gold (100), (110), (111), (211), and (311) faceted surfaces at top, long bridge, short bridge, and hole sites using a hybrid functional, so that they are directly comparable. Overall, most surfaces show preferential adsorption on top of surface atoms, with the most favorable adsorption at the top site of the (100) surface. The CO disproportionation activation energies on each surface are directly calculated to capture the complex interplay of electronic effects. The barriers are within ~ 1 eV of each other, with the lowest activation energy predicted for the (211) short bridge sites. In general, the less dense, higher

index facets promote both good adsorption and reactivity. The (311)/(311) and (110)/(100) edges both showed the lowest reaction barriers overall confirming that the experimental reactivity of the edges is from both higher LSP energies based on the shape of the particle and the open coordination of the edge atoms.

Acknowledgements

We acknowledge financial support from Lehigh University and research computing resources were provided by Lehigh University partially supported by the NSF CC* Compute program through Grant No. OAC-2019035 and TG-CHE190011 allocation from Extreme Science and Engineering Discovery Environment (XSEDE), which is supported by National Science Foundation Grant No. ACI-1548562.

References

- [1] W.-C.D. Yang, C. Wang, L.A. Fredin, P.A. Lin, L. Shimomoto, H.J. Lezec, R. Sharma, Site-selective CO disproportionation mediated by localized surface plasmon resonance excited by electron beam, Nat Mater 18 (2019) 614–619. https://doi.org/10.1038/s41563-019-0342-3.
- [2] A.A. Vedyagin, I. V Mishakov, P.G. Tsyrulnikov, The features of the CO disproportionation reaction over iron-containing catalysts prepared by different methods, Reaction Kinetics, Mechanisms and Catalysis 117 (2015) 35–46. https://doi.org/10.1007/s11144-015-0936-y.
- [3] G. Lanzani, A.G. Nasibulin, K. Laasonen, E.I. Kauppinen, CO dissociation and CO+O reactions on a nanosized iron cluster, Nano Res 2 (2009) 660–670. https://doi.org/10.1007/s12274-009-9069-9.
- [4] D.E. Jiang, E.A. Carter, Adsorption and dissociation of CO on Fe (1 1 0) from first principles, Surf Sci 570 (2004) 167–177. https://doi.org/10.1016/j.susc.2004.07.035.
- [5] D.E. Jiang, E.A. Carter, Effects of alloying on the chemistry of CO and H2S on Fe surfaces, Journal of Physical Chemistry B 109 (2005) 20469–20478. https://doi.org/10.1021/jp052656q.
- [6] D.E. Jiang, E.A. Carter, Prediction of a highly activated state of CO adsorbed on an Al/Fe(100) bimetallic surface, Journal of Physical Chemistry B 110 (2006) 22213–22219. https://doi.org/10.1021/jp056123t.

- [7] S. Sharifzadeh, P. Huang, E. Carter, Embedded configuration interaction description of CO on Cu(111): Resolution of the site preference conundrum, Journal of Physical Chemistry C 112 (2008) 4649–4657. https://doi.org/10.1021/jp710890a.
- [8] M. Kogler, E.M. Köck, B. Klötzer, T. Schachinger, W. Wallisch, R. Henn, C.W. Huck, C. Hejny, S. Penner, High-Temperature Carbon Deposition on Oxide Surfaces by CO Disproportionation, Journal of Physical Chemistry C 120 (2016) 1795–1807. https://doi.org/10.1021/acs.jpcc.5b12210.
- [9] W.J. Evans, M.J. Lipp, C.S. Yoo, H. Cynn, J.L. Herberg, R.S. Maxwell, M.F. Nicol, Pressure-induced polymerization of carbon monoxide: Disproportionation and synthesis of an energetic lactonic polymer, Chemistry of Materials 18 (2006) 2520–2531. https://doi.org/10.1021/cm0524446.
- [10] S. Mukherjee, F. Libisch, N. Large, O. Neumann, L. V Brown, J. Cheng, J.B. Lassiter, E.A. Carter, P. Nordlander, N.J. Halas, Hot electrons do the impossible: plasmon-induced dissociation of H2 on Au, Nano Lett 13 (2013) 240–247. https://doi.org/10.1021/nl303940z.
- [11] L. Zhou, C. Zhang, M.J. McClain, A. Manjavacas, C.M. Krauter, S. Tian, F. Berg, H.O. Everitt, E.A. Carter, P. Nordlander, N.J. Halas, Aluminum nanocrystals as a plasmonic photocatalyst for hydrogen dissociation, Nano Lett 16 (2016) 1478–1484. https://doi.org/10.1021/acs.nanolett.5b05149.
- [12] K.A. Willets, R.P. Van Duyne, Localized Surface Plasmon Resonance Spectroscopy and Sensing, Annu Rev Phys Chem 58 (2007) 267–297. https://doi.org/10.1146/annurev.physchem.58.032806.104607.
- [13] S. Linic, U. Aslam, C. Boerigter, M. Morabito, Photochemical transformations on plasmonic metal nanoparticles, Nat Mater 14 (2015) 567–576. https://doi.org/10.1038/nmat4281.
- [14] G. V Hartland, L. V Besteiro, P. Johns, A.O. Govorov, What's so hot about electrons in metal nanoparticles?, ACS Energy Lett 2 (2017) 1641–1653. https://doi.org/10.1021/acsenergylett.7b00333.
- [15] M.J. Kale, T. Avanesian, P. Christopher, Direct photocatalysis by plasmonic nanostructures, ACS Catal 4 (2014) 116–128. https://doi.org/10.1021/cs400993w.
- [16] I.X. GREEN, W. TANG, M. NEUROCK, J.T.JR. YATES, Spectroscopic Observation of DualCatalytic Sites During Oxidation of CO on a Au/TiO2 Catalyst, Science (1979) 333 (2011) 736–740. https://doi.org/10.1126/science.1207272.
- [17] Z.-P.P. Liu, P. Hu, A. Alavi, Catalytic Role of Gold in Gold-Based Catalysts: A Density Functional Theory Study on the CO Oxidation on Gold, J Am Chem Soc 124 (2002) 14770–14779. https://doi.org/10.1021/ja0205885.
- [18] M. Mavrikakis, P. Stoltze, J.K. Nørskov, Making gold less noble, Catal Letters 64 (2000) 101–106. https://doi.org/10.1023/A:1019028229377.

- [19] N. Lopez, T.V.W. Janssens, B.S. Clausen, Y. Xu, M. Mavrikakis, T. Bligaard, On the origin of the catalytic activity of gold nanoparticles for low-temperature CO oxidation, 223 (2004) 232–235. https://doi.org/10.1016/j.jcat.2004.01.001.
- [20] A. Hussain, D. Curulla Ferré, J. Gracia, B.E. Nieuwenhuys, J.W. Niemantsverdriet, DFT study of CO and NO adsorption on low index and stepped surfaces of gold, Surf Sci 603 (2009) 2734–2741. https://doi.org/https://doi.org/10.1016/j.susc.2009.07.023.
- [21] B. Assadollahzadeh, P. Schwerdtfeger, A systematic search for minimum structures of small gold clusters Au[sub n] (n=2-20) and their electronic properties, J Chem Phys 131 (2009) 064306. https://doi.org/10.1063/1.3204488.
- [22] J. Wang, M. McEntee, W. Tang, M. Neurock, A.P. Baddorf, P. Maksymovych, J.T. Yates, Formation, Migration, and Reactivity of Au-CO Complexes on Gold Surfaces, J Am Chem Soc 138 (2016) 1518–1526. https://doi.org/10.1021/jacs.5b09052.
- [23] W.-L. Yim, T. Nowitzki, M. Necke, H. Schnars, P. Nickut, J. Biener, M.M. Biener, V. Zielasek, K. Al-Shamery, T. Klüner, M. Bäumer, Universal Phenomena of CO Adsorption on Gold Surfaces with Low-Coordinated Sites, The Journal of Physical Chemistry C 111 (2007) 445–451. https://doi.org/10.1021/jp0665729.
- [24] N. Lopez, T.V.W. Janssens, B.S. Clausen, Y. Xu, M. Mavrikakis, T. Bligaard, On the origin of the catalytic activity of gold nanoparticles for low-temperature CO oxidation, 223 (2004) 232–235. https://doi.org/10.1016/j.jcat.2004.01.001.
- [25] D. Loffreda, P. Sautet, First-principles study of CO adsorption and vibration on Au surfaces, Journal of Physical Chemistry B 109 (2005) 9596–9603. https://doi.org/10.1021/jp050473y.
- [26] J.L.C. Fajín, M.N.D.S. Cordeiro, J.R.B. Gomes, DFT study of the CO oxidation on the Au(321) surface, Journal of Physical Chemistry C 112 (2008) 17291–17302. https://doi.org/10.1021/jp8031435.
- [27] A.M. Pessoa, J.L.C. Fajín, J.R.B. Gomes, M.N.D.S. Cordeiro, Ionic and radical adsorption on the Au(hkl) surfaces: A DFT study, Surf Sci 606 (2012) 69–77. https://doi.org/10.1016/j.susc.2011.08.023.
- [28] P. Giannozzi, S. Baroni, N. Bonini, M. Calandra, R. Car, C. Cavazzoni, D. Ceresoli, G.L. Chiarotti, M. Cococcioni, I. Dabo, A. Dal Corso, S. de Gironcoli, S. Fabris, G. Fratesi, R. Gebauer, U. Gerstmann, C. Gougoussis, A. Kokalj, M. Lazzeri, L. Martin-Samos, N. Marzari, F. Mauri, R. Mazzarello, S. Paolini, A. Pasquarello, L. Paulatto, C. Sbraccia, S. Scandolo, G. Sclauzero, A.P. Seitsonen, A. Smogunov, P. Umari, R.M. Wentzcovitch, QUANTUM ESPRESSO: a modular and open-source software project for quantum simulations of materials, Journal of Physics: Condensed Matter 21 (2009) 395502. https://doi.org/10.1088/0953-8984/21/39/395502.
- [29] A. Cao, J.K. Nørskov, Spin Effects in Chemisorption and Catalysis, ACS Catal 13 (2023) 3456–3462. https://doi.org/10.1021/acscatal.2c06319.

- [30] J.P. Perdew, K. Burke, M. Ernzerhof, Generalized Gradient Approximation Made Simple, Phys Rev Lett 77 (1996) 3865–3868. https://doi.org/10.1103/PhysRevLett.77.3865.
- [31] P.E. Blöchl, Projector augmented-wave method, Phys Rev B 50 (1994) 17953–17979. https://doi.org/10.1103/PhysRevB.50.17953.
- [32] J. Heyd, G.E. Scuseria, M. Ernzerhof, Hybrid functionals based on a screened Coulomb potential, Journal of Chemical Physics 118 (2003) 8207–8215. https://doi.org/10.1063/1.1564060.
- [33] J. Heyd, G.E. Scuseria, M. Ernzerhof, Erratum: "Hybrid functionals based on a screened Coulomb potential" [J. Chem. Phys. 118, 8207 (2003)], 124 (2006) 219906. https://doi.org/10.1063/1.2204597.
- [34] G. Henkelman, B.P. Uberuaga, H. Jónsson, Climbing image nudged elastic band method for finding saddle points and minimum energy paths, Journal of Chemical Physics 113 (2000) 9901–9904. https://doi.org/10.1063/1.1329672.
- [35] G. Henkelman, H. Jónsson, Improved tangent estimate in the nudged elastic band method for finding minimum energy paths and saddle points, Journal of Chemical Physics 113 (2000) 9978–9985. https://doi.org/10.1063/1.1323224.
- [36] G. Kresse, J. Furthmüller, Efficient iterative schemes for \textit{ab initio} total-energy calculations using a plane-wave basis set, Phys Rev B 54 (1996) 11169–11186.
- [37] P.E. Blöchl, Projector augmented-wave method, Phys Rev B 50 (1994) 17953–17979. https://doi.org/10.1103/PhysRevB.50.17953.
- [38] V. Wang, N. Xu, J.C. Liu, G. Tang, W.T. Geng, VASPKIT: A user-friendly interface facilitating high-throughput computing and analysis using VASP code, Comput Phys Commun 267 (2021) 108033. https://doi.org/10.1016/j.cpc.2021.108033.
- [39] Z.-P.P. Liu, P. Hu, A. Alavi, Catalytic Role of Gold in Gold-Based Catalysts: A Density Functional Theory Study on the CO Oxidation on Gold, J Am Chem Soc 124 (2002) 14770–14779. https://doi.org/10.1021/ja0205885.
- [40] M. Mavrikakis, P. Stoltze, J.K. Nørskov, Making gold less noble, Catal Letters 64 (2000) 101–106. https://doi.org/10.1023/A:1019028229377.
- [41] A. Hussain, D. Curulla Ferré, J. Gracia, B.E. Nieuwenhuys, J.W. Niemantsverdriet, DFT study of CO and NO adsorption on low index and stepped surfaces of gold, Surf Sci 603 (2009) 2734–2741. https://doi.org/https://doi.org/10.1016/j.susc.2009.07.023.
- [42] D. Loffreda, P. Sautet, First-principles study of CO adsorption and vibration on Au surfaces, Journal of Physical Chemistry B 109 (2005) 9596–9603. https://doi.org/10.1021/jp050473y.
- [43] J.L.C. Fajín, M.N.D.S. Cordeiro, J.R.B. Gomes, DFT study of the CO oxidation on the Au(321) surface, Journal of Physical Chemistry C 112 (2008) 17291–17302. https://doi.org/10.1021/jp8031435.

- [44] Z. Zeng, J. Greeley, Theoretical study of CO adsorption on Au catalysts under environmental catalytic conditions, Catal Commun 52 (2014) 78–83. https://doi.org/10.1016/j.catcom.2014.03.016.
- [45] S. Vijay, T. V. Hogg, J. Ehlers, H.H. Kristoffersen, Y. Katayama, Y. Shao Horn, I. Chorkendorff, K. Chan, B. Seger, Interaction of CO with Gold in an Electrochemical Environment, Journal of Physical Chemistry C 125 (2021) 17684–17689. https://doi.org/10.1021/acs.jpcc.1c04013.
- [46] M. Kuwahara, L. Mizuno, R. Yokoi, H. Morishita, T. Ishida, K. Saitoh, N. Tanaka, S. Kuwahara, T. Agemura, Transient electron energy-loss spectroscopy of optically stimulated gold nanoparticles using picosecond pulsed electron beam, Appl Phys Lett 121 (2022). https://doi.org/10.1063/5.0108266.
- [47] G. Ouyang, K.J. Zhu, L. Zhang, P.F. Cui, B.T. Teng, X.D. Wen, Effects of coordination number of Au catalyst on oxygen species and their catalytic roles, Appl Surf Sci 387 (2016) 875–881. https://doi.org/10.1016/j.apsusc.2016.07.027.
- [48] N. Lopez, J.K. Nørskov, Catalytic CO oxidation by a gold nanoparticle: A density functional study, J Am Chem Soc 124 (2002) 11262–11263. https://doi.org/10.1021/ja026998a.
- [49] G.D. Barmparis, I.N. Remediakis, Dependence on CO adsorption of the shapes of multifaceted gold nanoparticles: A density functional theory, Phys Rev B Condens Matter Mater Phys 86 (2012) 1–7. https://doi.org/10.1103/PhysRevB.86.085457.
- [50] S. Linic, U. Aslam, C. Boerigter, M. Morabito, Photochemical transformations on plasmonic metal nanoparticles, Nat Mater 14 (2015) 567–576. https://doi.org/10.1038/nmat4281.
- [51] G. V Hartland, L. V Besteiro, P. Johns, A.O. Govorov, What's so hot about electrons in metal nanoparticles?, ACS Energy Lett 2 (2017) 1641–1653. https://doi.org/10.1021/acsenergylett.7b00333.
- [52] M.J. Kale, T. Avanesian, P. Christopher, Direct photocatalysis by plasmonic nanostructures, ACS Catal 4 (2014) 116–128. https://doi.org/10.1021/cs400993w.